Journal of Catalysis **198,** 89–96 (2001)
doi:10.1006/jcat.2000.3112, available online at http://www.idealibrary.com on IDEAL®

n-Pentane Isomerization over $Pt/WO_x/ZrO_2$ Catalysts: A ^1H and ^{13}C NMR Study

S. V. Filimonova,* A. V. Nosov,* M. Scheithauer,† and H. Knözinger†,[1]

*Boreskov Institute of Catalysis, Lavrentieva, 5, Novosibirsk 630090, Russia; and †Department Chemie, Physikalische Chemie, Universität München, Butenandstrasse 5-13 (Haus E), D-81377, Münich, Germany

Received July 23, 2000; revised October 24, 2000; accepted October 28, 2000; published online February 8, 2001

The skeletal isomerization of *n*-pentane over platinum-promoted tungstated zirconia has been studied by the ^1H and ^{13}C nuclear magnetic resonance technique. $Pt/WO_x/ZrO_2$ samples with varying Pt concentrations have been used as catalysts. ^{13}C-labeled *n*-pentane was used to analyze the isotopic label distribution in the reaction products. A few aspects of the mechanism of *n*-pentane isomerization are discussed. Spectroscopic evidence was obtained indicating that initially *n*-pentane isomerization proceeds by a monomolecular pathway, most probably on Lewis acid sites, which permit hydride abstraction from *n*-alkane molecules. At higher conversion degrees, isopentane is produced both mono- and bimolecularly via oligomerization and β-fission of a chemisorbed C_{10}-carbenium ion. © 2001 Academic Press

Key Words: **isomerization; *n*-pentane; platinum on WO_x/ZrO_2; tungstated zirconia; NMR (^1H and ^{13}C); isotope labeling.**

INTRODUCTION

Zirconia-supported tungsta materials have attracted considerable attention (1–6) as promising catalysts for isomerization and alkylation reactions of light paraffins. These materials have been shown to exhibit increased isoparaffin selectivity and catalytic stability as compared to sulfated zirconia catalysts. Several aspects of WO_x/ZrO_2 materials (WZ) have been examined previously, namely the influences of the preparation method and of tungsta loading on catalytic performance (1–4), the reducibility of tungsten oxospecies (2, 3), tungstate structure (2, 5–7), and surface acidity (3–7).

The activity of WZ showed a strong dependence on the tungsten loading (passing through a maximum at approximately monolayer WO_3 loading) and consequently on the nature of tungsten oxide species present on the ZrO_2 surface (3, 4). Highly distorted octahedrally coordinated polytungstate species were assumed to provide catalytically active structures (2, 4–6). The octahedral polymeric WO_x clusters have been suggested to exist in a form of surface pseudoheteropolyacid with the possibility of mobile protons being incorporated in the WO_x network (4, 6). These protons were assumed to be responsible for the observed Brønsted acidity of tungstated zirconias. Surface acid sites in WO_x/ZrO_2 appear to be nonuniform. Catalytic titration experiments using 2,6-dimethylpyridine revealed a distribution of proton sites in WO_x/ZrO_2, the strong site density which is considered to be responsible for the high *n*-alkane isomerization activity being rather low (3). Coordinatively unsaturated surface Zr^{4+} ions interacting with nearby polytungstate species via inductive effects were assumed to provide the Lewis acidity of the materials (4, 6). According to Hino and Arata (1) and Ji *et al.* (7), specially prepared WO_x/ZrO_2 can develop a very strong acidity. However, recent infrared studies of CO adsorption (4, 6) did not reveal extremely acidic sites in WO_x/ZrO_2 catalysts and, thus, these systems were regarded as moderately strong solid acids.

Promotion with platinum improves the stability, activity, and selectivity of zirconia-supported tungsten oxide in isomerization of both light (C_4–C_6) and also of larger alkanes such as *n*-heptane (2, 8–13). Platinum-containing tungstated zirconia, PtWZ, may be regarded as a bifunctional metal–acid catalyst which combines an acid component with noble metal particles (2). Pt would promote the alkene formation, thus supporting the bifunctional mechanism of isomerization, namely dehydrogenation of an *n*-alkane to an alkene on the metallic function in the first step, followed by isomerization of the alkene on acid sites with subsequent hydrogenation of isoalkene (14). On the other hand, the Pt function may also create Brønsted acid sites by hydrogen spillover from metallic particles (2). The effects of Pt loading and of the preparative conditions of PtWZ catalysts on *n*-alkane isomerization activity and selectivity were discussed earlier in Refs. (9–12).

Recent infrared studies on low-temperature adsorbed CO (15) showed that the acid strength of surface sites on PtWZ is similar to that of unmodified tungstated zirconia. The Lewis and Brønsted acidity of PtWZ does not exceed that of zeolitic acids and of sulfated zirconias. The higher isomerization activity of PtWZ is, therefore, not only caused

[1] To whom correspondence should be addressed.

0021-9517/01 $35.00
Copyright © 2001 by Academic Press
All rights of reproduction in any form reserved.

by the acid strength. Consistent with this observation, a recent calorimetry study by Vartuli *et al.* (16) indicated no correlation between the acidity of WZ and *n*-alkane isomerization activity.

Mechanistic studies of the alkane isomerization over oxide-promoted ZrO_2 catalysts have been reported elsewhere (14, 17–22). The nature of the cationic intermediates has also been discussed. There is good experimental evidence that skeletal isomerization of *n*-butane takes place via a bimolecular mechanism involving oligomerization and β-fission of C_8-carbenium ions, thus avoiding the formation of a primary carbenium ion intermediate (17, 19, 20). For *n*-pentane, both mono- and bimolecular pathways were suggested (22). Monomolecular isomerization of *n*-pentane was supposed to proceed on Lewis acid sites (LAS), whereas the bimolecular mechanism requires Brønsted acid sites (BAS) for the formation of surface alkenes (22). ^{13}C NMR studies using labeled hydrocarbons have been used previously to study acid-catalyzed hydrocarbon reactions (23–25).

In the present investigation we contribute to the mechanistic studies of skeletal *n*-pentane isomerization over Pt-promoted WZ catalysts, in order to contribute to the clarification of the reaction mechanism. The relationship between the isomerization activity and the acid strength of the materials is also discussed. ^{13}C-labeled *n*-pentane CH_3–$^{13}CH_2$–$(CH_2)_2$–CH_3 was used to reveal the predominant reaction path.

EXPERIMENTAL

Sample Preparation

The details of the preparation of WZ materials have been reported previously (4, 6).

The WO_x/ZrO_2 sample (19.0 wt% WO_3, surface area 96 $m^2 \cdot g^{-1}$) was prepared by suspending hydrous zirconium oxide (MEL Chemicals, Manchester) in an aqueous solution of ammonium metatungstate ($(NH_4)_6[H_2W_{12}O_{40}] \cdot nH_2O$, Fluka) at the natural pH. The suspension was refluxed at 383 K for 16 h followed by drying at 383 K for 12 h and calcination at 923 K for 3 h (2.5 K/min). The Pt-containing catalysts with three different platinum loadings (0.3, 1.0, and 3.0 wt%) were prepared by incipient wetness impregnation of the calcined WO_x/ZrO_2 with a solution of $Pt(NH_3)_4(NO_3)_2$ in water followed by drying at 383 K for 12 h and calcination at 823 K.

NMR Measurements

The ^1H and ^{13}C NMR magic angle spinning (MAS) technique was used to identify the catalytic properties of the WZ and PtWZ and to elucidate the distribution of reaction products in the *n*-pentane skeletal isomerization.

The NMR spectra were taken on a Bruker MSL-400 spectrometer operating at a magnetic field of 9.4 T (resonance frequencies are 400.1 and 100.6 MHz for the ^1H and ^{13}C nuclei, respectively). Magic angle spinning (MAS) was performed using sealed sample tubes in the quartz Andrew Beams rotor (26) at a rotation frequency of 3.0–3.5 kHz.

A pulse width of 5 μs and recycle time of 3 s were applied to accumulate 100 scans of the ^1H MAS NMR spectra. The ^1H chemical shifts (ppm) were referenced to an external tetramethylsilane standard within an accuracy of ± 0.2 ppm. ^{13}C NMR spectra were recorded with 5 μs radio frequency pulses and a recycle delay of 3 s. The total number of accumulations varied from 500 to 1000. Broad band decoupling was employed. ^{13}C chemical shifts were referenced to an external tetramethylsilane standard. In several cases, cross-polarization experiments (contact time 5 ms) combined with MAS (denoted below as ^{13}C CP/MAS NMR) were performed.

Prior to the adsorption of *n*-pentane, the samples (typically ca. 0.35 g) were placed into glass sample tubes (outer diameter 7 mm, length 12 mm), evacuated to about 10^{-3} Pa at 673 K (1 K/min) over 2–3 h, reduced in H_2 (5×10^4 Pa, 673 K) for 30 min, and finally evacuated at 673 K for about 20 min. A fixed, volumetrically measured amount of *n*-C_5H_{12} (100 μmol/g) was adsorbed on the pretreated sample, and then the sample tube was sealed off and kept in liquid nitrogen until ^1H and ^{13}C NMR measurements were started.

Typically, before the measurements, the sealed NMR tube with adsorbed *n*-pentane was heated to a selected temperature and maintained at this temperature for a given time. The NMR spectrum was taken after quenching of the sample to 293 K; after that the sample was returned to the chosen reaction conditions and heated for longer periods of time.

Isotopically enriched *n*-pentane CH_3–$^{13}CH_2$–$(CH_2)_2$–CH_3 (99%) with the ^{13}C isotope selectively in the $C^{(2)}$ position (2^*C_5) was used in the experiments.

RESULTS AND DISCUSSION

^1H NMR

^1H NMR chemical shifts for *n*-pentane are 0.9–1.0 ppm (CH_3 groups) and 1.3–1.4 ppm (CH_2 groups), with the relative integral intensities of the corresponding lines being 6 : 6 (24). CH_3 and $CH + CH_2$ protons of isopentane would give ^1H resonance peaks at nearly the same positions as the protons of CH_3 and CH_2 groups of *n*-pentane, respectively (24). Hence, quantitative conversion of *n*-pentane to isopentane would result in an increase of the signal intensity at 0.9–1.0 ppm by a factor of 1.5 (protons of CH_3 groups) and in a 2-fold decrease of the intensity of the line at 1.3–1.4 ppm (protons of $CH + CH_2$ groups).

At room temperature neither WZ nor PtWZ catalysts showed detectable isomerization activity. On PtWZ catalysts the reaction started at about 373 K under our experimental conditions, as indicated by the redistribution of

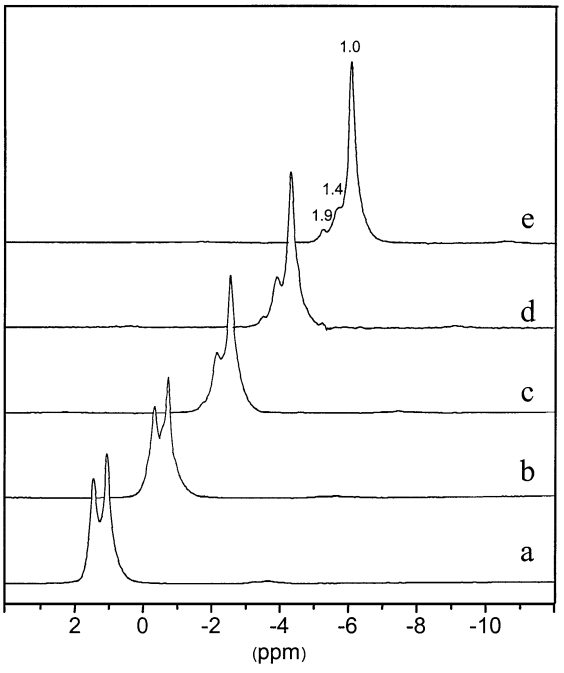

FIG. 1. ^{1}H MAS NMR spectra produced by the adsorption of *n*-pentane on 1.0% Pt/WO_x/ZrO_2: at room temperature (a) and after heating of the sample at 373 K for 15 min (b), 30 min (c), 60 min (d), and 90 min (e).

the ^{1}H NMR signal intensities after *n*-pentane adsorption. In contrast, for the platinum-free samples, no detectable changes in the ^{1}H signal intensities of *n*-C_5H_{12} were found up to 373 K. Higher temperatures were required to initiate the reaction on these materials. The difference in isomerization activity between WZ and PtWZ catalysts (about 10–20 times) was also observed in catalytic tests at 525 K in the presence of H_2 (27).

Representative ^{1}H MAS NMR results for the 1.0% Pt/WO_x/ZrO_2 sample are shown in Fig. 1. As can be seen, the intensity of the ^{1}H NMR peak of CH_2 protons of *n*-pentane (1.4 ppm) decreases in the course of the reaction, while the peak of CH_3 protons (1.0 ppm) grows in intensity. In addition, a weak signal due to disproportionation products appears at higher conversion degrees at 1.9 ppm.

n-Pentane adsorbed on the WO_x/ZrO_2 samples with 0.3 and 3.0 wt% Pt produced similar ^{1}H NMR spectra (not shown).

The poorly resolved low-field peak at about 1.9 ppm (spectra c, d, and e in Fig. 1) corresponds to the protons of the CH groups of isobutane (23b) (the latter is formed as a side product at early stages of the reaction, as will be shown below) and also to the protons of the CH fragments of aliphatic C_6 hydrocarbons which might be formed together with isobutane. The appearance of isobutane means that the protons of its methyl groups together with the protons of methyl groups of C_6 compounds contribute to the ^{1}H resonance peak at 1.0 ppm, while the protons of methylene groups of C_6 compounds would contribute to the peak at 1.4 ppm (23b). This contribution from side products does not allow us to evaluate quantitative parameters of *n*-pentane conversion from the analysis of the ^{1}H resonance peak intensities (as has been done, e.g., in Ref. (24)); i.e., in the present case such an analysis would be incorrect. Note that the intensity of the ^{1}H resonance peak at 1.9 ppm can serve only as a rough approximation of the relative amount of the side products formed, since due to its broadening it does not quantitatively correspond to their content (the latter will be confirmed below by the ^{13}C NMR results).

Since only limited information on the reaction products can be obtained from the ^{1}H NMR data, we have performed ^{13}C NMR studies to detect the product distribution in more details.

^{13}C NMR

More details on hydrocarbon surface species (and possible reaction intermediates) can be derived from the analysis of the ^{13}C NMR spectra produced by adsorption of ^{13}C-labeled *n*-pentane onto the Pt/WO_x/ZrO_2 catalysts. In our experiments, we used *n*-pentane selectively enriched with the ^{13}C isotope in the $C^{(2)}$ position (2^*C_5). This allowed us to monitor the redistribution of the ^{13}C isotope label in the reaction products.

As an example, Fig. 2 illustrates ^{13}C MAS NMR spectra of *n*-pentane adsorption on the Pt/WO_x/ZrO_2 catalyst with 1.0 wt% Pt loading. The ^{13}C resonance line of the $C^{(2)}$ atom of *n*-pentane was detected at $\delta = 22.9$ ppm in the spectrum recorded immediately after adsorption at room temperature (Fig. 2, spectrum a). After heating of the sample at 373 K for 10 min, isopentane labeled in both the $C^{(2)}$ (30.3 ppm) and $C^{(3)}$ (32.0 ppm) positions was formed (Fig. 2, spectrum b). Also coinciding resonances of CH and CH_3 groups of isobutane (23.8 ppm) appeared in the spectrum. Only a very small amount of isopentane containing labeled methyl groups 1^*iC_5 and 4^*iC_5 ($C^{(1)}$ and $C^{(4)}$ carbons resonating at 21.3 and 11.1 ppm, respectively) was detected at the beginning of the reaction. The appearance of a weak signal at 13.1 ppm of CH_3 groups of *n*-pentane should also be noted (Fig. 2, spectra a and b), indicating the migration of the ^{13}C isotope label from a CH_2 group of the *n*-pentane molecule into the neighboring methyl group. At higher conversion characterized by a decreased intensity of the resonance line of *n*-pentane (22.9 ppm) (heating the sample at 373 K for 20 min, Fig. 2, spectrum c), the peaks of isopentane 1^*iC_5 (21.3 ppm) and 4^*iC_5 (11.1 ppm) show significant growth. Resonances of isopentane 2^*iC_5 and 3^*iC_5 (30.3 and 32.0 ppm) also continue to grow in intensity. At much higher conversion (Fig. 2, spectrum d), numerous side products were detected, of which isobutane (23.8 ppm) is the main one. Among other side products, propane (15.2 and 16.2 ppm), *n*-butane (25.5 ppm), and C_6

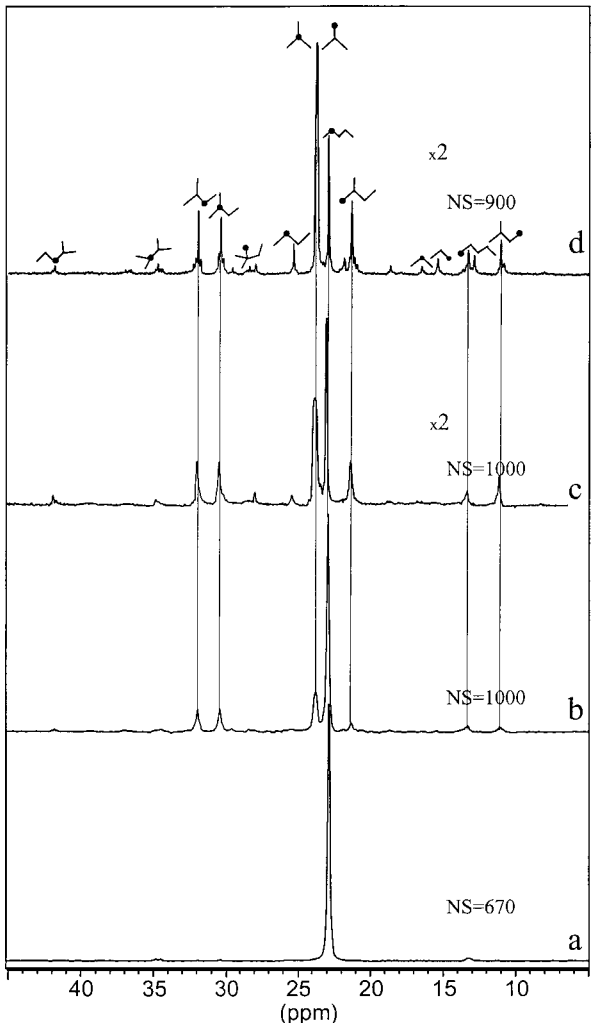

FIG. 2. ^{13}C MAS NMR spectra produced by the adsorption of *n*-pentane on 1.0% $Pt/WO_x/ZrO_2$: at room temperature (a) and after heating of the sample at 373 K for 10 min (b), at 373 for 20 min (c), and at 423 K for 5 min (d).

compounds (dimethylbutanes, 28.0, 34.6 ppm; methylpentane, 41.8 ppm) were observed in smaller amounts.

It should be noted that factors such as mobility and relaxation times affect the relative intensity of the ^{13}C NMR signals of the various CH_n groups. The ^{13}C carbon balance shows that in some cases not all carbon atoms are detected; i.e., part of the ^{13}C nucleus becomes "NMR-invisible." As can be seen in Fig. 2, when the ^{13}C resonance peak of isobutane appears (spectrum b), the signals from other side products that are formed together with isobutane (e.g., C_3, C_6 compounds) are broadened beyond the detection limit and become detectable only at the later stages of the reaction (spectra c and d of Fig. 2). Thus, some loss of quantitative information may occur. Nevertheless, the analysis of the ^{13}C NMR spectra allows us to derive valuable information regarding the product distribution in the isomerization reaction of *n*-pentane. Here and below we will be concentrating on the analysis of the distribution of the various labeled isopentane products, based on a reasonable assumption that relaxation affects their signals in all samples in the same way.

First, we will estimate the isomerization activity of the $Pt/WO_x/ZrO_2$ catalysts (373 K) using the change of the ^{13}C resonance signal intensity of *n*-pentane. The activity, *A*, is defined as the absolute amount of *n*-pentane transformed into isopentane and other products per time unit (*t*):

$$A = (n_0 - n)/t, \text{ or}$$

$$A = [I_0(nC_5) - I(nC_5)]/t.$$

Here n_0 and n are the amounts of *n*-pentane prior to the reaction and after time *t*, while $I_0(nC_5)$ and $I(nC_5)$ are the corresponding ^{13}C peak intensities. Using the time interval of 20 min for the 1 wt% $Pt/WO_x/ZrO_2$ catalyst (Figs. 2a–2c), we estimate the activity value of $A = (3.2 \pm 0.2) \times 10^{-6}$ mol · min^{-1} · g^{-1}.

The same procedure for the $Pt/WO_x/ZrO_2$ catalysts with 0.3 and 3.0 wt% Pt gives $A = (2.7 \pm 0.2) \times 10^{-6}$ mol · min^{-1} · g^{-1} (0.3% Pt) and $A = (3.8 \pm 0.2) \times 10^{-6}$ mol · min^{-1} · g^{-1} (3.0% Pt). Thus, the PtWZ materials with higher Pt loadings showed the higher activities, although the activity increase is not proportional to the Pt concentration. The estimated *A* values are lower than those previously found for sulfated zirconias from ^1H NMR data (room temperature) (24).

An interesting conclusion follows from the analysis of the ^{13}C NMR spectra. In the initial stages of the reaction (Fig. 2, spectrum b), isopentane labeled predominantly in the $C^{(2)}$ and $C^{(3)}$ positions was formed, the rate of formation of isopentane 1^*iC_5 and 4^*iC_5 being much lower. The observed scrambling of the ^{13}C isotope label in the *n*-pentane molecule should also be pointed out.

The different formation rates of the ^{13}C-labeled isopentane products are illustrated in Fig. 3, showing the time dependencies of their integral NMR intensities in the course of the reaction of *n*-pentane. The initial formation rate of isopentane 1^*iC_5 and 4^*iC_5 is several times lower than that of isopentane 2^*iC_5 and 3^*iC_5. Note that the difference between curves b and c in Fig. 3 (both in the slope and in the *Y*-axis value) is due to the difference in numbers of $C^{(1)}$ and $C^{(4)}$ carbons in the isopentane molecule.

The experimentally observed distribution of the ^{13}C-labeled products can be explained if the reaction scheme shown in Fig. 4 is accepted. According to this scheme, initially a secondary cation C_5^+ (**1**) is produced. In principle, carbenium ions can be formed either via hydride abstraction from an *n*-alkane molecule over a Lewis acid site (LAS), or via H^+ addition to the C–H bond of alkane on Brønsted acid sites (BAS) followed by H_2 elimination (Olah mechanism) (28). The presently proposed scheme suggests the former pathway, namely the H^- transfer from *n*-pentane

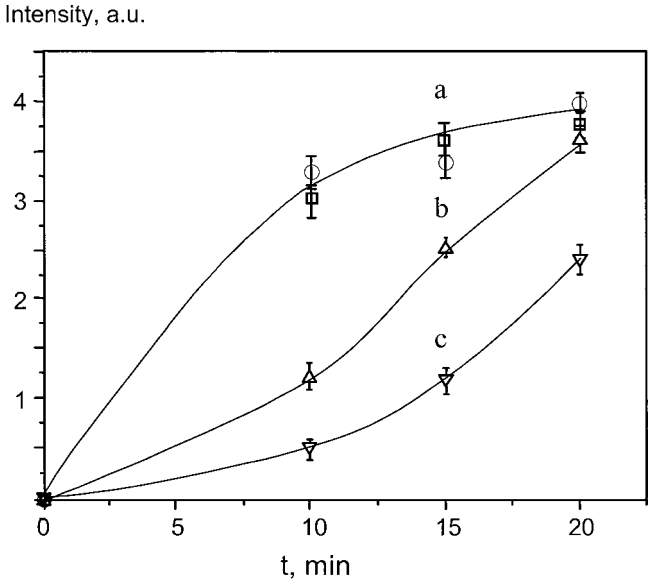

FIG. 3. Time courses of the integral intensities of the ^{13}C NMR peaks of different labeled isopentane products over 1.0% $Pt/WO_x/ZrO_2$ at 373 K: 2^*iC_5 (a, circles), 3^*iC_5 (a, squares), 1^*iC_5 (b), and 4^*iC_5 (c).

to a LAS (or to another carbenium ion), although the role of BAS cannot be completely excluded. Carbenium ion **1** is then transformed into a methyl-substituted cyclopropyl cation (**2**), which has been proposed elsewhere to describe the distribution of products in the acid-catalyzed reactions of hydrocarbons (29). Cation **2** is easily converted into the cations **3** and **4**, which are the precursors of isopentane labeled in the $C^{(2)}$ and $C^{(3)}$ positions. Both were visible in the ^{13}C NMR spectra at the beginning of the reaction in amounts considerably exceeding those of iospentane labeled in the methyl groups, 1^*iC_5 and 4^*iC_5 (Fig. 2, spectrum b; Fig. 3). This suggests that the monomolecular pathway of *n*-pentane isomerization, proceeding via cation **2** (Fig. 4), dominates in the initial stages of the reaction. At higher conversion degrees, however, isopentane labeled in the methyl groups (21.3 and 11.1 ppm) appears in relatively large amounts (Fig. 2, spectrum c). There are two possibilities for its formation, namely (i) a monomolecular pathway (not shown in the scheme) involving cation **5**, and/or (ii) a bimolecular pathway occurring via dimeric C_{10}^+ species formed from C_5^+ and an alkene $C_5^=$, followed by the rearrangement of these C_{10}^+ intermediates and their cracking to C_4–C_6 products (Fig. 4). The former process should be energetically unfavorable because of the formation of a primary cation from **5**. Nevertheless, cation **5** is most certainly formed at low conversions in the course of the reaction, along with cation **2**, as indicated by the observed migration of the ^{13}C isotope label in *n*-pentane molecules to the $C^{(1)}$ position at 13.1 ppm (Fig. 2, spectrum b), proceeding only via **5**, according to the scheme. One can estimate the approximate ratio between the concentrations of cations [**2**] to [**5**], by using the sum of integral intensities of the signals of the $CH + CH_2$ carbons of isopentane 2^*iC_5 (30.3 ppm) and 3^*iC_5 (32.0 ppm) formed via **2**, divided by twice the intensity of the line of *n*-pentane labeled in the methyl groups (13.1 ppm) formed via **5** (Fig. 2, spectrum c):

$$[\mathbf{2}]/[\mathbf{5}] = (I(\mathrm{CH}) + I(\mathrm{CH_2}))/2I(\mathrm{CH_3}) \geq 10.$$

Thus, the isomerization of *n*-pentane proceeding via cation **5** (yielding isopentane 1^*iC_5 and 4^*iC_5) should be about 1 order of magnitude slower than the pathway involving cyclopropyl cation **2**. Nevertheless, at higher conversions (ca. 75%, Fig. 2, spectrum c), isopentane 1^*iC_5 and 4^*iC_5 appear in larger amounts than would be expected if the above-mentioned path via **5** was the only possible one. Obviously, the bimolecular reaction involving C_{10}^+ dimers which give isopentane 1^*iC_5 and 4^*iC_5 (Fig. 4) becomes prevailing at higher degrees of *n*-pentane conversion. Cracking products C_3–C_6 (e.g., propane, isobutane, dimethylbutanes) detected at the end of the reaction (Fig. 2, spectrum d) could be formed both via cracking of C_{10}^+ species (Fig. 4) and also via the side reactions involving isoalkanes.

Thus we infer that both mono- and bimolecular pathways are feasible in the course of *n*-pentane isomerization. The former one, involving most probably the methyl-substituted cyclopropyl cation (**2**), dominates in the initial stages. It gives no side products and leads to high selectivity to isopentane. At higher conversions, both mono- and bimolecular processes become possible. Bimolecular reaction involves C_{10}^+ dimers undergoing subsequent isomerization and β-fission responsible for the C_4–C_6 products and for reduced selectivity of the reaction. In this stage, isopentane is formed via C–C fission of these C_{10}^+ dimeric intermediates (Fig. 4).

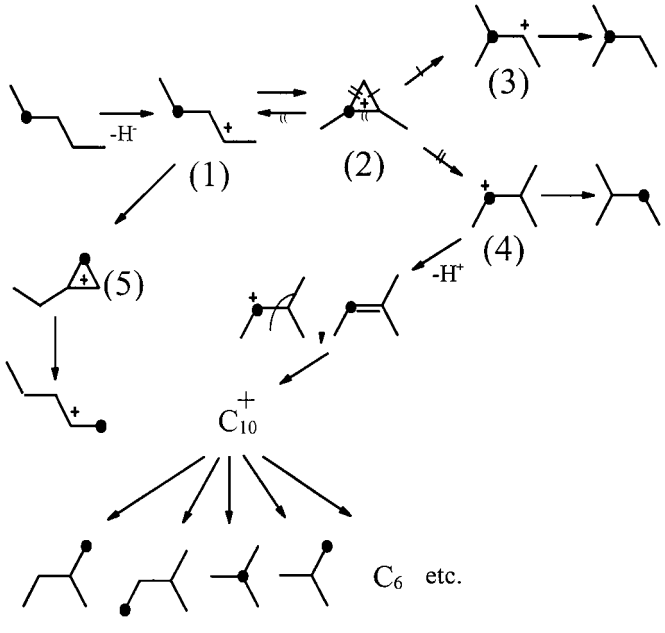

FIG. 4. Scheme of *n*-pentane conversion over $Pt/WO_x/ZrO_2$.

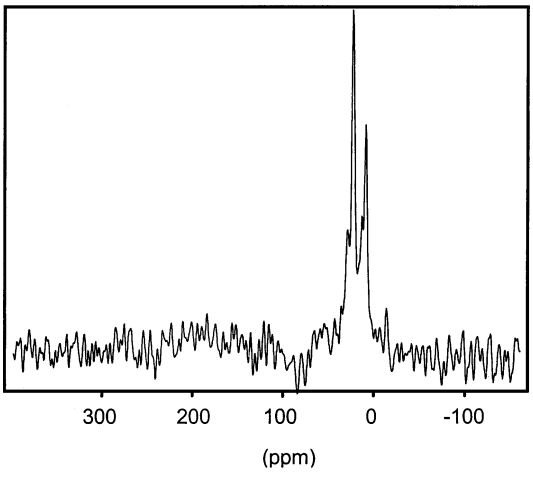

FIG. 5. ^{13}C CP MAS NMR spectrum of 1.0% $Pt/WO_x/ZrO_2$ after exposure to *n*-pentane.

In principle, cycloalkyl cations formed in the course of hydrocarbon reactions can be detected by solid-state NMR (25, 30). Usually, to detect (strongly adsorbed) species of low mobility, the cross-polarization (CP) technique in combination with MAS is used. In this type of experiment the signal strength is enhanced due to a polarization transfer from abundant (^1H) to rare spins (^{13}C) by using special pulse sequences (31, 32). Note that since a number of factors (relaxation phenomena, the distances between the ^1H and ^{13}C nuclei, etc.) affect the extent of polarization, a perturbation in the relative intensities of the ^{13}C resonances occurs in the CP experiment (32); i.e., the ^{13}C peak intensities often do not correspond to the contents of the various CH_n groups.

The ^{13}C CP/MAS NMR spectrum of *n*-pentane on 1 wt% $Pt/WO_x/ZrO_2$ is illustrated in Fig. 5. Carbon atoms in the carbenium ion center of the methyl-substituted cyclopropyl cation (**2**) could be visible between 200 and 250 ppm (25). Nevertheless, no signals were detected in this region (Fig. 5) when *n*-pentane was contacted with PtWZ, most probably because of the high reactivity (low stability) of these intermediate species, or because of the significant line broadening caused by the presence of neighboring paramagnetic species (e.g., W^{5+}). The intense broad peaks centered at about 10 and 25 ppm in Fig. 5 overlap with the narrow signals from highly mobile aliphatic species which were clearly observed in Fig. 2. We can not unambiguously decide to which species (aliphatic and/or olefinic) the broad resonance lines in Fig. 5 correspond. In principle, C_4–C_6 alkenes would be visible at 12–25 and 125–131 ppm (23a), and thus, olefinic products might contribute to the peak centered at about 10 ppm in the ^{13}C CP/MAS NMR spectra of Fig. 5. On the other hand, since such species seem to be highly reactive and thus to have low surface concentrations they also might not be detected in NMR experiments of this type (33) because of the rapid secondary reactions leading to heavier products with low mobility, the resonances of which are broadened beyond the detection limit.

The accumulation of alkenes as intermediate species has been previously attributed to the occurrence of the induction period in alkane isomerization over tungstated zirconia catalysts (4, 14). Alkenes could then contribute to a bimolecular pathway leading to an increased isomerization rate. Although we were not able to obtain unambiguous evidence for alkene formation from the ^{13}C NMR spectra, such a possibility cannot be excluded. Another possible reason for the observed induction period could be an accumulation of the reduced W^{5+} species which were supposed to play an important role in isomerization reactions of alkanes (15).

There is still little agreement in the literature as to whether Brønsted or Lewis acid sites are responsible for the isomerization activity of oxide-promoted ZrO_2 catalysts. For sulfated zirconias, both Brønsted (18) and Lewis acid sites (21, 24, 34) were supposed to be important. Some cooperative action between these two types of sites has also been proposed (35). The behavior of the PtWZ materials cannot be ascribed to a simple combination of a metallic function and a strongly acidic support (14). Tungsta species may induce electronic and/or morphological modifications of Pt particles (36), while Pt is known to strongly influence the reducibility of W species (2). Although significant differences in acid strength between WO_x/ZrO_2 and $Pt/WO_x/ZrO_2$ catalysts were not found (15), they did not show identical catalytic behavior in the *n*-pentane isomerization. The calculated activity values increased with increasing Pt loading on WO_x/ZrO_2, while for the catalysts without platinum no activity could be detected under similar conditions (373 K). This indicates that not only do tungsta species provide acid function, but also platinum contributes to the observed isomerization activity of PtWZ. The better activity of PtWZ was previously attributed to the ability of platinum (i) to activate an acid function by spillover of hydrogen adatoms from metal sites to WO_x species and (ii) to assist in the hydrogen-transfer reaction and carbocation desorption (2).

It is important to point out that the effect of Pt on *n*-pentane isomerization was observed in the absence of hydrogen in the present study. We may speculate that H_2 chemisorbed on metallic Pt^0 particles during hydrogen reduction (before isomerization) is not removed completely during short evacuation. And thus, H^+ sites could have been formed from H atoms stored by Pt^0 centers. The newly formed proton sites in PtWZ presumably arising from increased generation of H^+ species by hydrogen spillover from Pt^0 (the first possible role of Pt) have recently been detected by ^1H NMR (15). The possible role of BAS would be an increased formation of carbonium ions which can be then transformed into carbenium ions by H_2 elimination. The latter can either contribute to a monomolecular

pathway, or convert into an alkene which is an intermediate in the bimolecular reaction.

However, according to recent IR data (15), the strength of BAS in PtWZ is not unusually high and, thus, these centers probably cannot simply account for the observed activity increase. A more reasonable explanation of the role of Pt might be an enhanced dehydrogenation reaction of *n*-alkane resulting in alkene formation which can either be isomerized on the acid site with subsequent hydrogenation giving isoalkane (14), or react with a C_5^+ intermediate according to the bimolecular isomerization mechanism (Fig. 4).

High *n*-pentane isomerization activity requires the presence of Pt clusters of an intermediate size. A recent HREM study showed that the cluster size of metallic Pt species on PtWZ increases from ca. 0.5 nm for 1.0% Pt to ca. 5 nm for 3.0% Pt loading (37). For the sample with 0.3% Pt loading, no clusters were visible, indicating the Pt particle size to be less than 0.5 nm. The isomerization activity is not directly proportional to the Pt cluster size: the largest cluster size was found in the sample with 3.0% Pt loading, and it showed an activity which was only slightly higher than that for the 1.0% Pt sample. The possible reason for this could be decreased total metal surface area in the sample with the highest Pt loading. Thus, metallic particles with an optimum size which provides high dispersion of Pt should exist for developing high isomerization activity of PtWZ.

We may expect that Pt not only (i) increases formation of BAS and (ii) promotes dehydrogenation reactions, but also (iii) influences the nature and the number of LAS, since it is known to promote the reducibility of tungsta species (2). The strength of LAS in PtWZ is not changed dramatically as compared to unmodified WZ, as indicated by CO infrared band shifts as observed for low-temperature CO adsorption (15). LAS in both WZ and PtWZ are not superacidic; at least they are less acidic than those found in sulfated zirconia materials (24). In SZ catalysts, hydride abstraction from *n*-alkane over LAS was supposed to occur in an initial step of the isomerization reaction (21). We may speculate that H^- abstraction could also be the reason for *n*-alkane activation over PtWZ (Fig. 4). Those LAS could be both Zr^{4+} and also W^{6+} and W^{5+} species. The W^{5+} centers appear in WZ during hydrogen reduction of the samples (15). In the presence of Pt, W^{6+} species start to reduce already at room temperature by H atom diffusion from Pt sites to WO_x (38). The reduced W^{5+} centers are also formed in the course of the isomerization of *n*-pentane, as has been suggested previously by several authors (2, 38) and experimentally proved in (15). Slight reduction of the W^{6+} centers in WO_x clusters promoted by the presence of Pt might provide an increase in the density of Lewis acid sites in PtWZ and consequently an increase of its isomerization activity.

On the other hand, the formation of W^{5+} species under these reaction conditions (*n*-pentane, 523 K) (15) may suggest a one-electron transfer between the alkane molecule and the catalyst surface, i.e. activation of *n*-alkane through a redox process. For sulfated zirconias, the one-electron oxidation of the hydrocarbon by sulfate species to a carbocation precursor was supposed to initiate the isomerization reaction (39). In tungstated zirconias, the redox properties of WO_x species may also play an important role in the activation of the alkane. Carbenium ions which are then formed due to a second electron transfer are stabilized by the $H_2^+W_{n-2}^{6+}W_2^{5+}O_{3n}$ centers by charge compensation (38). So we may speculate that one of the possible reasons for the higher isomerization activity of PtWZ as compared to unpromoted WZ might be an increased contribution of the activation of *n*-alkane through a redox process, as inferred from increased concentration of the reduced W^{5+} centers in PtWZ formed in the course of *n*-alkane reaction, as indicated by ESR experiments (15).

Another possibility for the initation of the isomerization reaction could be hydride transfer from *n*-alkane molecules to isomerized carbocations; i.e., the process required for the desorption of isoalkane formed (species **3** and **4** in the scheme of Fig. 4). In this case, alkane isomerization would proceed via a chain-transfer pathway, in which carbenium ions propagate by hydrogen transfer from neutral alkane molecules to the isomerized carbocations (40).

An unambiguous answer as to which process of the initiation of the isomerization reaction is preferable (related to LAS or to the formation of W^{5+} species which might be responsible for the one-electron oxidation of *n*-alkane) is not available at the moment. Further studies are required to clarify the mechanism of generation of the initial isomerization activity of tungstated zirconia materials.

CONCLUSIONS

Platinum-promoted WO_x/ZrO_2 catalysts exhibit much higher activities in *n*-pentane isomerization as compared to unpromoted WO_x/ZrO_2. Activities measured by ^{13}C NMR were found to increase with increasing Pt content on tungstated zirconia, indicating that not only the acidic functions are important for the isomerization reaction. An intermediate cluster size of metallic Pt species is required for high isomerization activity. The role of Pt might be both dehydrogenation activity (increased alkene formation and promotion of bimolecular isomerization mechanism) and increased BAS generation. Both these contributions might be important for developing the isomerization activity of PtWZ, although the importance of the latter contribution remains still questionable since BAS in PtWZ materials seems not to be strong enough to be able to protonate *n*-alkanes. The Pt promoter does not dramatically change the strength of LAS, which is not unusually high in tungstated zirconias. Addition of platinum promotes the reducibility of WO_x species, resulting in the creation of W^{5+} centers

which may act as Lewis acid sites and which also stabilize carbocationic intermediates. LAS might be responsible for the initial high activity of the PtWZ materials provided hydride abstraction from *n*-alkane molecule plays a crucial role. On the other hand, the isomerization reaction can also be initiated by a one-electron transfer between the alkane molecule and the catalyst surface, as can be inferred from the formation of the reduced W^{5+} species during the isomerization process (2, 15, 38). Increased concentration of the reduced W^{5+} centers formed in the presence of Pt (15) might be one of the reasons for the higher isomerization activity of PtWZ as compared to unpromoted WZ. Further studies are needed to give an answer as to whether the Lewis acidity or redox properties of the WO_x species are responsible for the initiation of the isomerization reactions of *n*-alkanes over tungstated zirconias.

Our ^{13}C NMR study of products distribution and identification of the primary labeled products show that both mono- and bimolecular pathways of *n*-pentane skeletal isomerization may occur. The former dominates in the initial stages of the reaction and proceeds most probably via the formation of cyclopropyl cation species. It then changes to a bimolecular pathway which gives relatively large amounts of cracking products.

ACKNOWLEDGMENTS

The authors gratefully acknowledge Dr. D. A. van Langeveld and S. Kuba for valuable discussions. The international collaboration was financially supported by the Deutsche Forschungsgemeinschaft (SFB 338).

REFERENCES

1. Hino, M., and Arata, K., *J. Chem. Soc., Chem. Commun.* 1259 (1987).
2. Iglesia, E., Barton, D. G., Soled, S. L., Miseo, S., Baumgartner, J. E., Gates, W. E., Fuentes, G. A., and Meitzner, G. D., *Stud. Surf. Sci. Catal.* **101**, 533 (1996).
3. Santiesteban, J. G., Vartuli, J. C., Han, S., Bastian, R. D., and Chang, C. D., *J. Catal.* **168**, 431 (1997).
4. Scheithauer, M., Cheung, T.-K., Jentoft, R. E., Grasseli, R. K., Gates, B. C., and Knözinger, H., *J. Catal.* **180**, 1 (1998).
5. (a) Boyse, R. A., and Ko, E. I., *J. Catal.* **171**, 191 (1997). (b) Boyse, R. A., and Ko, E. I., *Appl. Catal. A: General* **177**, L131 (1999).
6. Scheithauer, M., Grasseli, R. K., and Knözinger, H., *Langmuir* **14**, 3019 (1998).
7. Ji, W., Hu, J., and Chen, Y., *Catal. Lett.* **53**, 15 (1998).
8. Soled, S. L., AlChE 1994 Annual Meeting, paper 85f, San Francisco, November 1994.
9. Larsen, G., Lotero, E., and Parra, R. D., *Stud. Surf. Sci. Catal.* **101**, 543 (1996).
10. Larsen, G., and Petkovic, L. M., *Appl. Catal. A: General* **148**, 155 (1996).
11. Vaudagna, S. R., Comelli, R. A., and Fígoli, N. S., *Appl. Catal. A: General* **164**, 265 (1997).
12. Vaudagna, S. R., Canavese, S. A., Comelli, R. A., and Fígoli, N. S., *Appl. Catal. A: General* **168**, 93 (1998).
13. Barton, G., Soled, S. L., Meitzner, G. D., Fuentes, G. A., and Iglesia, E., *J. Catal.* **181**, 57 (1999).
14. Yori, J. C., Pieck, C. L., and Parera, J. M., *Appl. Catal. A: General* **181**, 5 (1999).
15. Kuba, S., Concepción Heydorn, P., Grasselli, R. K., Gates, B. C., Che, M., and Knözinger, H., *Phys. Chem. Chem. Phys.* **3**, 146 (2001).
16. Vartuli, J. C., Santiesteban, J. G., Traverso, P., Cardona-Martinez, N., Chang, C. D., and Stevenson, S. A., *J. Catal.* **187**, 131 (1999).
17. Adeeva, V., Lei, G. D., and Sachtler, W. M. H., *Appl. Catal. A: General* **118**, L11 (1994).
18. Garin, F., Seyfried, L., Girard, P., Maire, G., Abdulsamad, A., and Sommer, J., *J. Catal.* **151**, 26 (1995).
19. Yaluris, G., Larson, R. B., Kobe, J. M., Gonzalez, M. R., Fogash, K. B., and Dumesic, J. A., *J. Catal.* **158**, 336 (1996).
20. Sommer, J., Jost, R., and Hachoumy, M., *Catal. Today* **38**, 309 (1997).
21. Coman, S., Pârvulescu, V., Grange, P., and Parvulescu, V. I., *Appl. Catal., A: General* **176**, 45 (1999).
22. Matsuhashi, H., Shibata, H., Nakamura, H., and Arata, K., *Appl. Catal., A: General* **187**, 99 (1999).
23. (a) Stepanov, A. G., Luzgin, M. V., Romannikon, V. N., and Zamaraev, K. I., *Catal. Lett.* **24**, 271 (1994); (b) Luzgin, M. V., Stepanov, A. G., Sassi, A., and Sommer, J., *Chem. Eur. J.* **6**, 2368 (2000).
24. Mastikhin, V. M., Nosov, A. V., Filimonova, S. V., Terskikh, V. V., Kostsarenko, N. S., Shmachkova, V. P., and Kim, V. I., *J. Mol. Catal. A: Chemical* **101**, 81 (1995).
25. Knözinger, H., *Topics Catal.* **6**, 107 (1998).
26. Mastikhin, V. M., Mudrakovsky, I. L., and Nosov, A. V., *Prog. NMR Spectrosc.* **23**, 259 (1991).
27. Scheithauer, M., Ph.D. thesis, Universität München, 1998.
28. Cheung, T.-K., Lange, F. C., and Gates, B. C., *Catal. Lett.* **34**, 351 (1995).
29. Poutsma, M. L., *in* "Zeolite Chemistry and Catalysis" (J. A. Rabo, Ed.), pp. 437–528. Am. Chem. Soc., Washington, DC, 1976.
30. Haw, J. F., Nicholas, J. D., Xu, T., Beck, L. W., and Ferguson, D. B., *Acc. Chem. Res.* **29**, 259 (1996).
31. Pines, A., Gibby, M. G., and Waugh, J. S., *J. Chem. Phys.* **59**, 569 (1973).
32. Burum, D. P., *in* "Encyclopedia of NMR" (D. M. Grant and R. K. Harris, Eds.), pp. 1535–1542. Wiley, New York, 1996.
33. Ivanova, I. I., Rebrov, A. I., Pomakhina, E. B., and Derouane, E. G., *J. Mol. Catal. A: Chemical* **141**, 1107 (1999).
34. Morterra, C., Cerrato, G., Pinna, F., Signoretto, M., and Strukul, G., *J. Catal.* **149**, 181 (1994).
35. Ward, D. A., and Ko, E. I., *J. Catal.* **150**, 18 (1994).
36. Contreras, J. L., and Fuentes, G. A., *Stud. Surf. Sci.* **101**, 1195 (1996).
37. Kooyman, P. J., and van Langeveld, D. A., Delft University of Technology, personal communication (in preparation).
38. Barton, D. G., Soled, S. L., and Iglesia, E., *Topics Catal.* **6**, 87 (1998).
39. Fârcasiu, D., Ghenciu, A., and Li, J. Q., *J. Catal.* **158**, 116 (1996).
40. Iglesia, E., Soled, S. L., and Kramer, G. M., *J. Catal.* **144**, 238 (1993).